Biomaterials

International Edition: DOI: 10.1002/anie.201502485
German Edition: DOI: 10.1002/ange.201502485

Self-(Un)rolling Biopolymer Microstructures: Rings, Tubules, and Helical Tubules from the Same Material**

*Chunhong Ye, Svetoslav V. Nikolov, Rossella Calabrese, Amir Dindar, Alexander Alexeev, Bernard Kippelen, David L. Kaplan, and Vladimir V. Tsukruk**

Abstract: *We have demonstrated the facile formation of reversible and fast self-rolling biopolymer microstructures from sandwiched active–passive, silk-on-silk materials. Both experimental and modeling results confirmed that the shape of individual sheets effectively controls biaxial stresses within these sheets, which can self-roll into distinct 3D structures including microscopic rings, tubules, and helical tubules. This is a unique example of tailoring self-rolled 3D geometries through shape design without changing the inner morphology of active bimorph biomaterials. In contrast to traditional organic-soluble synthetic materials, we utilized a biocompatible and biodegradable biopolymer that underwent a facile aqueous layer-by-layer (LbL) assembly process for the fabrication of 2D films. The resulting films can undergo reversible pH-triggered rolling/unrolling, with a variety of 3D structures forming from biopolymer structures that have identical morphology and composition.*

Inspired by the activated shape changes of plant organs found in nature, such as pine cones,[1] the Venus Flytrap,[2] or peapod valves,[3] various synthetic approaches have been pursued to design three-dimensional (3D) shapes that arise from the transformation of initial 2D planar films. In nature, it is common that fibrous tissues composed of long, narrow, and rigid fibers embedded in a soft, pliant matrix build up internal stresses as a result of differential swelling in response to changes of the ambient humidity, leading to different shapes.[4] To emulate such systems de novo, different experimental and theoretical designs utilize solid material patches connected by active hinges, which employ metal–metal, metal–polymer, polymer–polymer,[5,6] folding of the polymer films,[7] chemomechanical meditation of gel-embedded nanorod arrays,[8] or self-rolling of patterned hydrogel helical tubules.[9] Tailored interfacial stresses within bilayer structures were employed for the fabrication of large bendable planar structures.[10]

Various responsive soft materials and structures have been utilized as dynamic components for selective drug encapsulation and targeting,[11] energy harvesting and storage,[12] and actuating micro-robotic structures.[13] Such actuating and adaptive structures have been based on a wide range of responsive materials, mostly involving elastomeric synthetic gels, which are responsive to pH, temperature, light, humidity, ionic strength, and magnetic and electric fields.[14–16] However, for a variety of self-rolling and self-folding structures, careful tuning of composition, morphology, patterning schemes, and thicknesses of 2D templates is required. Intensive research has been directed to facilitate the formation of 3D structures, such as adaptive microcapsules, microchambers, or grippers[17–19] with prospective applications as microcarriers,[11] actuators,[13] micro-robots,[13] and bioscaffolds.[20]

Herein we demonstrate the rapid formation of novel microscopic self-rolling/unrolling biopolymer microstructures from small sandwiched active-passive, silk-on-silk materials that can roll themselves into different shapes. This self-rolling feature is controlled by "cutting" different shapes from the same photolithographically preformed sheets. In contrast to currently reported responsive structures usually fabricated on a large spatial scale (mm to cm), these silk-on-silk microscopic (20–100 μm) structures are assembled by facile aqueous-based LbL methods, and offer biocompatible and biodegradable structures. Furthermore, shape-controlled biaxial stress distribution in the silk-on-silk sheet structures initiates the formation of a variety of 3D shapes such as rings, tubules, and helical tubules with the same composition and morphology which are stable over a wide pH range, from acidic to basic conditions, for rolling/unrolling control.

In our approach, an active silk I layer is sandwiched with β-sheet (crystalline) silk II as a passive layer along with the polystyrene (PS) supporting layer by spin-assisted LbL assembly as described elsewhere (see Figure 1 a).[18,21] The active silk I (amorphous) multilayer is composed of bilayers of silk-poly(amino acid) ionomers, prepared by LbL assembly of chemically grafted silk fibroin backbones with poly-L-glutamic acid or poly-L-lysine (anionic ionomer: silk-poly-L-

[*] Dr. C. Ye, Prof. V. V. Tsukruk
School of Materials Science and Engineering
Georgia Institute of Technology
Atlanta, GA 30332 (USA)
E-mail: Vladimir@mse.gatech.edu
S. V. Nikolov, Prof. A. Alexeev
Woodruff School of Mechanical Engineering
Georgia Institute of Technology
Dr. R. Calabrese, Prof. D. L. Kaplan
Department of Biomedical Engineering, Tufts University
4, Colby street, Medford, MA 02155 (USA)
Dr. A. Dindar, Prof. B. Kippelen
School of Electrical and Computer Engineering
Georgia Institute of Technology

[**] We appreciate the assistance and helpful discussions from Sidney T. Malak, Kesong Hu, and Marius Chyasnavichyus. This work is supported the National Science Foundation grants CBET-1402712, DMR-1255288, and DMR-1505234, and the Air Force Office for Scientific Research awards FA9550-14-1-0269 and FA9550-14-1-0015.

Supporting information for this article is available on the WWW under http://dx.doi.org/10.1002/anie.201502485.

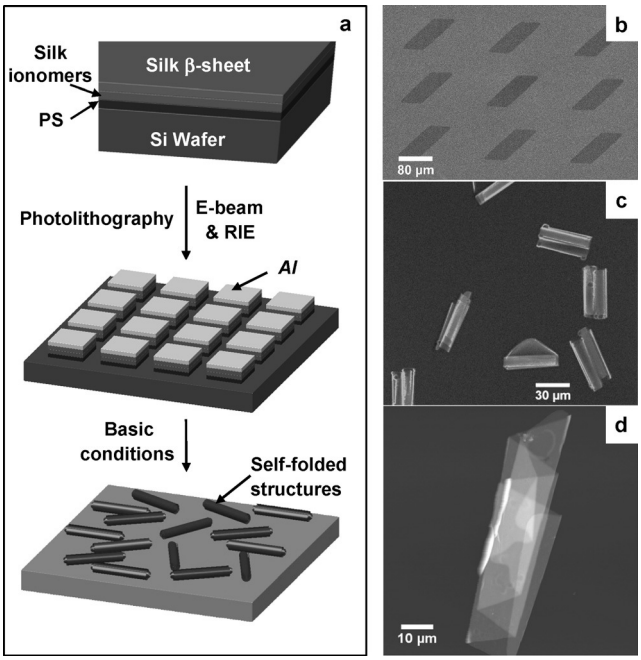

Figure 1. a) Fabrication of silk-on-silk structures; from top to bottom: sandwiched film formation, photolithographical patterning, etching, and release; b) SEM image of silk microsheet array; c) Confocal image of the silk microtubules labeled with fluorescein isothiocyanate (FITC); d) AFM image of a microtubule with helical morphology. E-beam = Electron-beam evaporator, RIE = plasma thermal reactive-ion etching.

glutamic acid, SF-PG and cationic ionomer: silk-poly-L-lysine, SF-PL), thus facilitating the conventional linear LbL growth. This assembly results in a $(SF\text{-}PG/SF\text{-}PL)_{12}$ silk film with total thickness from 42 nm to 49 nm for different specimens.[22] The passive silk II (partially crystallized) multilayer is prepared by partial transformation of silk fibroin random-coil molecular to ordered β-sheet domains by treatment with methanol to result in a stronger and insoluble silk material of the same nominal composition. These $(SF\text{-}PG/SF\text{-}PL)_{10}$ silk films possess a total thickness of 30–40 nm for different specimens.[23] A spin-cast PS layer ((65 ± 1) nm thickness for all specimens) acts as a supporting substrate on silicon as well as a supporting layer after release from the silicon wafer. The total thickness of these stable triple-layered structures varied between 140–160 nm. The silk materials were further cross-linked with 1-ethyl-3-[3-(dimethylamino)propyl]-carbodiimide hydrochloride (EDC) linker to provide the covalent bonds necessary for stability over a wide pH range, from 1.5 to 12.0 (see the Supporting Information).[24]

The sandwiched silk films were patterned by photolithography combined with dry etching to fabricate an array of microscopic silk sheets with "cuts" of preprogrammed dimensions and shapes (Figure 1a,b). The substrate with silk sheets was submerged into 0.06 mol L^{-1} NaOH solution that triggered the swelling of the active silk ionomer layer followed by release and self-rolling of all the triple-layered microsheets (Silk II–Silk I–PS) from the substrate, as confirmed by AFM cross-section profiles (Figure 1). Large-scale arrays of ultrathin (around 150 nm) silk sheets with precisely controlled shapes and micrometer lateral dimensions (20 μm to 100 μm) were prepared in this manner (one example is given in Figure 1b). The silk ionomer interlayer undergoes a significant swelling in the buffer solution because of the reduction in ionic bonding under extremely basic conditions,[25] while the physical crosslinked silk β-sheet layer remains unchanged at different pH values,[26] and the PS layer also maintains a constant volume, therefore, both layers functioned as "passive" layers. The high interfacial stress in this active–passive bimorph causes release of silk-on-silk sheets followed by their self-rolling into numerous different hollow tubular structures (Figure 1c,d). The shape of these self-rolled structures can be predictably controlled by "cutting" silk sheets into different shapes as discussed below.

A variety of parallelogram shapes were prepared for this study (Figure 2). The most intriguing finding was that silk sheets with fixed dimensions and different angles, 15°, 30°, and 90°, are transformed into very different 3D shapes such as rings, helical tubules, and conventional tubules, respectively (Figure 2b,e,h). The confocal images of the fluorescence-labeled sheets confirmed consistent 3D shapes of these self-

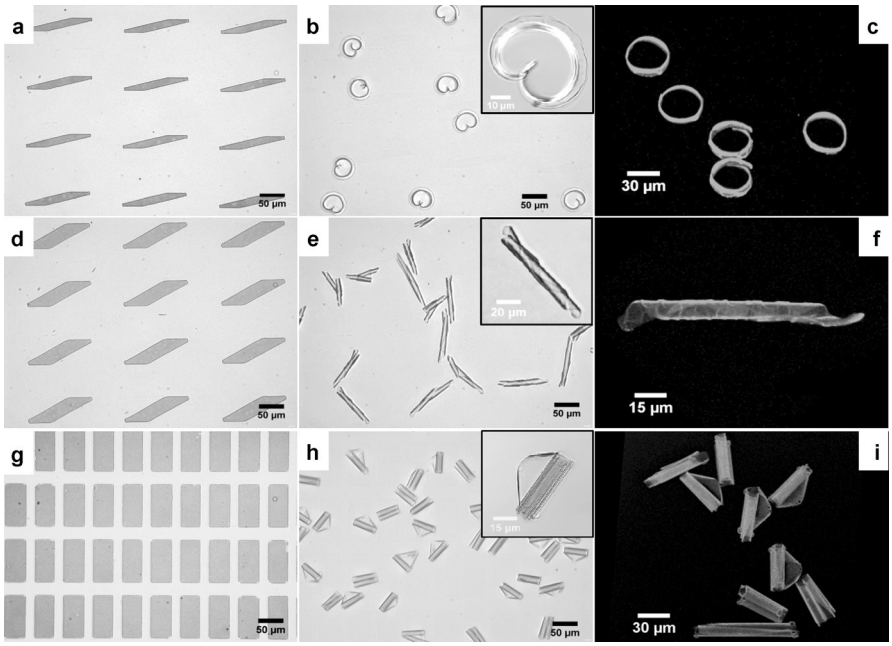

Figure 2. Self-rolling behavior for different silk–silk sheets: rings from 15° parallelograms (a–c); helical tubules from 30° parallelograms (d–f), and tubules from rectangular sheets (g–i). Lateral dimensions: 50×100 μm; specific thicknesses of different layers for these specimens are (67 ± 2) nm (PS), (45 ± 2) nm (active silk I), (30 ± 2) nm (passive silk II). Scale bars: 50 μm (a,b,d,e,g,h main images), 10 μm (b, inset), 20 μm (e, inset), 15 μm (h, inset).

rolled structures in solution (Figure 2c, f, i). The transformation from 2D sheets to 3D structures was very uniform with more than 95% microsheets self-rolled (from tens of thousands individual sheets at one wafer), and the vast majority of self-rolled structures (around 85%) formed identical morphologies.

In order to rationalize these dramatic differences in 3D shapes for identical inner morphologies, we analyzed interfacial stress fields in these structures. Indeed, according to the theory of stability of elastic plates under external stresses, the sandwiched sheets undergo bending (first-order buckling) if the interfacial stresses exceed a certain critical stress σ_{cr}, which is determined by the Young's modulus of materials, and the thickness and lateral dimensions of the plates.[27] However, for the complex triple-layer internal morphology of the structures studied here, simple analytical solutions are not adequate and computer modeling is required to understand the stress-field distributions. To this end, the lattice spring model (LSM) has been exploited for the analysis of the shape-dependent self-rolling behavior of these sheets.[28] In these simulations, we consider that the swelling of the active silk is constrained by the topmost passive silk II, in which the geometric constraints results in mismatched elastic strain and thus excessive interfacial stresses with non-uniform biaxial distribution along adjacent edges (Figure 3).

The simulation demonstrated that for parallelogram silk-on-silk sheets with shallow angles, the initial bending occurs at sharp angle corners while the opposite corners remain mostly flat (Figure 3b). A further increase in the interfacial stress resulted in symmetrical rolling of these corners until the sharp corners met each other, thus forming ringlike structures identical to those observed experimentally (Figure 3c, d). The same initial rolling behavior from minor angles was observed for 30° sheets (Figure 3f). However, the larger corners released from the substrate resulted in higher rolling compared to that of 15° parallelograms, attributed to the larger internal bending moment. Finally, the asymmetric rolling along the diagonal forced the 30° sheet to form a helical tubules (Figure 3g, h). For the 90° sheet, two orthogonal rolling directions were found. This behavior suggests two self-rolling directions are possible for rectangular sheets depending on their initial random deformations during release, which is in fact observed experimentally (Figure 3i–p) (for more details see the Supporting Information).

Finally, we explored the reversible self-rolling/unrolling behavior of the silk-on-silk sheets triggered by switching pH between basic (self-rolling initiated) to neutral (return to initial state) conditions. These changes were monitored in real time with confocal microscopy (Figure 4). It is worth noting that only the active silk ionomer layers with covalent cross-linking demonstrated stability during these transformations. This reversible behavior is driven by the volume expansion of the silk ionomers active layers under basic conditions, whereas the topmost silk β-sheet layer and supporting PS layer remain unchanged. The deprotonation of lysine groups on the poly-L-lysine modified silk above its pK_a (ca. 9) reduces ionic pairing constraints with the side poly-L-glutamic acid groups, resulted in the dramatic swelling/deswelling of this active silk ionomer layer as discussed previously.[22]

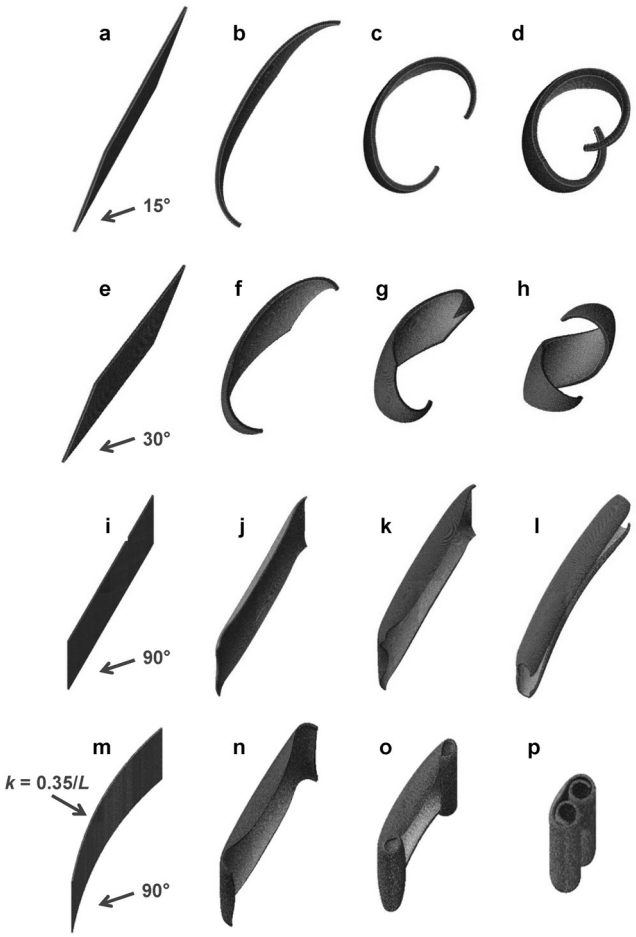

Figure 3. Simulated self-folding behavior of silk-on-silk sheets with different shapes at different rolling stages (from left to right). k = initial curvature, L = length of the microsheet.

Furthermore, the swelling behavior for the triple-layered sheet was determined by neutron reflectivity, and indicated that the thickness of the silk ionomers layer increased by a factor of four in basic condition, while the thickness of β-sheet silk film and PS support stay the same, as will be addressed in our future work.

In conclusion, we have demonstrated the formation of active self-rolling biopolymer 2D microstructures by using sandwiched active–passive silk-on-silk morphology. We experimentally showed and theoretically confirmed that the shape of individual sheets and biaxial stresses control the reversible self-rolling behavior and the formation of distinct 3D structures including rings, tubules, and helical tubules from the same 2D materials. This is a unique example of tailoring of self-rolled 3D geometries by "cutting" sheets of different shapes without changing the inner morphology of active materials.

In contrast to previously exploited synthetic organic-soluble gel bilayers with micrometer thickness and macroscopic lateral dimensions, these new self-rolled ultrathin sheets are based on biocompatible and biodegradable silk proteins materials by facile LbL assembly. We anticipate that further complexity in shapes could also be achieved by more

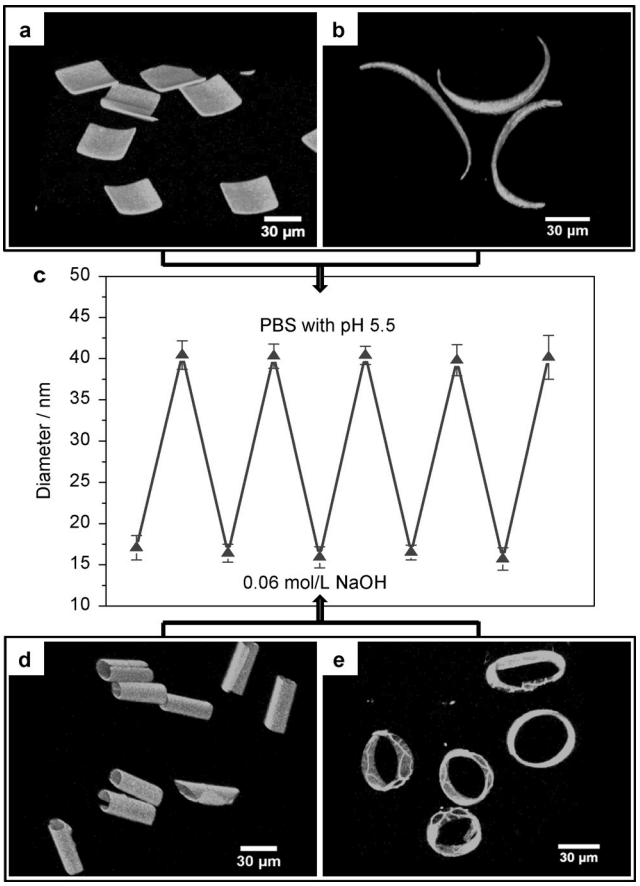

Figure 4. Reversible self-rolling/unrolling behavior of silk-on-silk sheets with various geometries (rectangular sheets shown in (a) and (d); 15° parallelograms shown in (b) and (e). a, b) CLSM images of reversible "opened" sheets at pH 5.5 and d, e) corresponding microtubules under basic conditions.

complex patterning of the individual sheets, and the scalability of the photolithography process will allow the fabrication of tens of millions of 3D structures in high yields. Moreover, these cytofriendly biopolymer structures with fully reversibly actuating behavior are extremely stable in harsh aqueous environments (extremes of pH, high ionic strength), which presents a promising platform for a wide range of applications such as drug delivery, active cell encapsulation, bioscaffolds, soft robotics, and biosensors.

Keywords: biomaterials · biopolymers · layer-by-layer assembly · microstructures · silk

How to cite: *Angew. Chem. Int. Ed.* **2015**, *54*, 8490–8493
Angew. Chem. **2015**, *127*, 8610–8613

[1] P. Fratzl, F. G. Barth, *Nature* **2009**, *462*, 442.
[2] Y. Forterre, J. M. Skotheim, J. Dumais, L. Mahadevan, *Nature* **2005**, *433*, 421.
[3] S. Armon, E. Efrati, R. Kupferman, E. Sharon, *Science* **2011**, *333*, 1726.
[4] L. D. Zarzar, P. Kim, J. Aizenberg, *Adv. Mater.* **2011**, *23*, 1442.
[5] J. S. Randhawa, M. D. Keung, P. Tyagi, D. H. Gracias, *Adv. Mater.* **2010**, *22*, 407.
[6] J. T. B. Overvelde, S. Shan, K. Bertoldi, *Adv. Mater.* **2012**, *24*, 2337.
[7] G. Stoychev, S. Turcaud, J. W. C. Dunlop, L. Ionov, *Adv. Funct. Mater.* **2013**, *23*, 2295.
[8] A. Grinthal, J. Aizenberg, *Chem. Soc. Rev.* **2013**, *42*, 7072.
[9] Z. L. Wu, M. Moshe, J. Greener, H. Therien-Aubin, Z. Nie, E. Sharon, E. Kumacheva, *Nat. Commun.* **2013**, *4*, 1586.
[10] L. Ionov, *Soft Matter* **2011**, *7*, 6786.
[11] B. Pokroy, S. H. Kang, I. Mahadevan, J. Aizenberg, *Science* **2009**, *323*, 237.
[12] J. Deng, H. Ji, C. Yan, J. Zhang, W. Si, S. Baunack, S. Oswald, Y. Mei, O. G. Schmidt, *Angew. Chem. Int. Ed.* **2013**, *52*, 2326; *Angew. Chem.* **2013**, *125*, 2382.
[13] E. W. H. Jager, O. Inganäs, I. Lundström, *Science* **2000**, *288*, 2335.
[14] A. Sidorenko, T. Krupenkin, A. Taylar, P. Fratzl, J. Aizenberg, *Science* **2007**, *315*, 487.
[15] B. Pokroy, A. K. Epstein, C. M. Persson-Gulda, J. Aizenberg, *Adv. Mater.* **2009**, *21*, 463.
[16] R. Geryak, J. Geldmeier, K. Wallace, V. V. Tsukruk, *Nano Lett.* **2015**, *15*, 2679.
[17] C. M. Andres, I. Larraza, T. Corrales, N. A. Kotov, *Adv. Mater.* **2012**, *24*, 4597.
[18] C. Ye, D. H. Kulkarni, H. Dai, V. V. Tsukruk, *Adv. Funct. Mater.* **2014**, *24*, 4364.
[19] S. Xu, Z. Yan, K.-I. Jang, W. Huang, H. Fu, J. Kim, Z. Wei, Y. Huang, Y. Zhang, J. A. Rogers, et al., *Science* **2015**, *347*, 154.
[20] E. Gultepe, J. S. Randhawa, S. Kadam, S. Yamanaka, F. E. Selaru, E. J. Shin, A. N. Kallo, D. H. Gracias, *Adv. Mater.* **2013**, *25*, 514.
[21] O. Shchepelina, I. Drachuk, M. K. Gupta, J. Lin, V. V. Tsukruk, *Adv. Mater.* **2011**, *23*, 4655.
[22] C. Ye, O. Shchepelina, R. Calabrese, I. Drachuk, D. L. Kaplan, V. V. Tsukruk, *Biomacromolecules* **2011**, *12*, 4319.
[23] C. Jiang, X. Wang, R. Gunawidjaja, Y.-H. Lin, M. K. Gupta, D. L. Kaplan, R. R. Naik, V. V. Tsukruk, *Adv. Funct. Mater.* **2007**, *17*, 2229.
[24] V. Kozlovskaya, E. Kharlampieva, M. L. Mansfield, V. Sukhishvili, *Chem. Mater.* **2006**, *18*, 328.
[25] C. Ye, I. Drachuk, C. Rossella, H. Dai, D. L. Kaplan, V. V. Tsukruk, *Langmuir* **2012**, *28*, 12235.
[26] H.-J. Jin, J. Park, V. Karageorgiou, U.-J. Kim, R. Valluzzi, P. Cebe, D. L. Kaplan, *Adv. Funct. Mater.* **2005**, *15*, 1241.
[27] S. P. Timoshenko, J. M. Gere, *Theory of Elastic Stability*, McGraw-Hill, Singapore, **1963**, p. 348.
[28] G. A. Buxton, C. M. Care, D. J. Cleaver, *Modell. Simul. Mater. Sci. Eng.* **2001**, *9*, 485.

Received: March 18, 2015
Revised: May 7, 2015
Published online: June 2, 2015

